C-A/AP/#128
December 2003

# Cold AGS Snake Optimization by Modeling

A.U. Luccio, R. Gupta, W.W. MacKay, T. Roser


**Collider-Accelerator Department**
**Brookhaven National Laboratory**
**Upton, NY 11973**

# Cold AGS Snake Optimization by Modeling

A.U. Luccio, R.Gupta, W.W.MacKay, T.Roser

December 23, 2003

## 1 A snake for the AGS

Acceleration of polarized protons in the AGS with minimum loss of polarization can be achieved by means of Siberian Snakes [1]. At the present time only one such snake is installed, consisting of a solenoid, that produces a spin rotation of about 9 degrees, (5% snake). In order to achieve a higher degree of polarization at extraction (the AGS accelerates protons from 1.2 GeV to 26 GeV), we plan to install a more powerful snake.

The space available in the machine for this insertion is about 2.6 m, then the new snake must be very compact. A possible structure for a compact and strong snake is obtained with an arrangement of helical dipoles that produce a transverse field whose direction rotates continuously around the axis of the magnet, as originally proposed by Ernest Courant. and has been built for RHIC, following a design proposed by Shatunov and Ptitsyn [2].

RHIC snakes are made of four 2.4 $m$ helical dipoles, and are are too long for the AGS. So, we have studied the possibily of building a compact helical snakes, with the helical pitch changing along the structure. Many ideas have been considereded, A compact four-helix structure, a two helix structure, a continuously varying pitch helix, and finally we decided on a scheme advertised by Thomas Roser [3], that consists of a sequence of three helices with different pitches. This structure appeared the most efficient in terms of spin rotation, orbit control and enginering.

We arrived at the final design of the magnetic field in the following steps: (i) Analytical modeling of the field of the snake, with calculation of orbit and spin propagation; (ii) Generation of numerical maps of the field with the code Opera-3D [4]; (iii) Fitting of the map with the model. Iterative optimization of the design using the model, with production at each step of an improved *Opera* map.

Two groups have been leading the effort in parallel, at Brookhaven, and at RIKEN, Japan, At BNL it was studied a practical implementation of a super conducting (cold, CS) 3-Tesla snake [5], and at RIKEN a similar design for a normal conducting (warm, WS) 1.5-Tesla snake [6]. Important differences between the two snakes -apart from the much larger spin rotation produced by the cold snake- are (i) in the CS the iron is saturated, then the field scales

almost linearly with the current in the coils, (ii) in the WS the field is not linear with the excitation, (iii) the CS must be operated in DC, (iv) in principle the current in the WS may be varied during the AGS cycle.

In this note we will limit ourselves to the description of the field modeling procedure, used to optimize both design. We will describe in detail the optimization of the cold snake, the more challenging of the two, mentioning only in passing the warm snake.

## 2 Basic structure of the snake. Field integrals

The spin of a proton moving in a magnetic field precesses and emerges at the end of the magnet with a different orientation, according to the BMT equation

$$\frac{d\vec{S}}{dt} = C_1[\vec{S} \times \vec{\Omega}] + C_2(\vec{\beta} \cdot \vec{\Omega})[\vec{S} \times \vec{\beta}], \quad C_1 = 1 + G\gamma, \quad C_2 = -\frac{G\gamma^2}{1+\gamma}, \tag{1}$$

where $G = g/2 - 1 = 1.7928$ is the reduced proton gyromagnetic costant. For an helical field the precession has been described by Ptitsyn and Shatunov [2], using a rotating coordinate frame.

After traversing the snake, the rotation of the spin is proportional to the integral of the absolute value of the field along the trajectory $I_s = \int |B| dz$. Integration of Eq.(1) shows that for a spin rotation of 45 deg (25% snake) the needed field integral is $\sim 4.5$ T-m, then, for a magnetic structure of effective length 1.5 m, a field of 3 T (cold snake). A 1.5 T snake (warm) may only produce a 22.5 deg rotation (12.5% snake).

In a helical field the orbit of a particle is also helical. For the orbit of the central particle of a beam traversing the snake we try to satisfy the following conditions: (i) In both transverse directions (x, horizontal and y, vertical) the exit orbit must be parallel to the orbit at the entrance, (ii) the orbit displacement at both ends should be the same, and (iii) both orbit angles and displacements should be zero. The above should possibly be met with no use of devices extenal to the snake.

Conditions (i,ii,iii) translate into conditions for the integrals of the components of the field (field integrals). This is easily seen as follows: since the curvature of the trajectory of a particle of momentum $p = eB\rho$ is just

$$y''(z) = \frac{1}{\rho_y} = \frac{e}{p} B_x(z), \quad x''(z) = \frac{1}{\rho_x} = -\frac{e}{p} B_y(z), \tag{2}$$

the angle and the trajectory are obtained by a first and second integration, in $y$ (and similarly in $x$)

$$y'(z) = y'_0 + \frac{e}{p} I_1^{(x)}(z), \quad y(z) = y_0 + y'_0 z + \frac{e}{p} I_2^{(x)}(z) \tag{3}$$

with the 1.st and 2.nd field integral (for $y$, and similarly for $x$ with a - sign) defined as

$$I_1^{(x)}(z) = \int_0^z B_x(z')dz', \quad I_2^{(x)}(z) = \int_0^z I_1^{(x)}(z')dz' \tag{4}$$

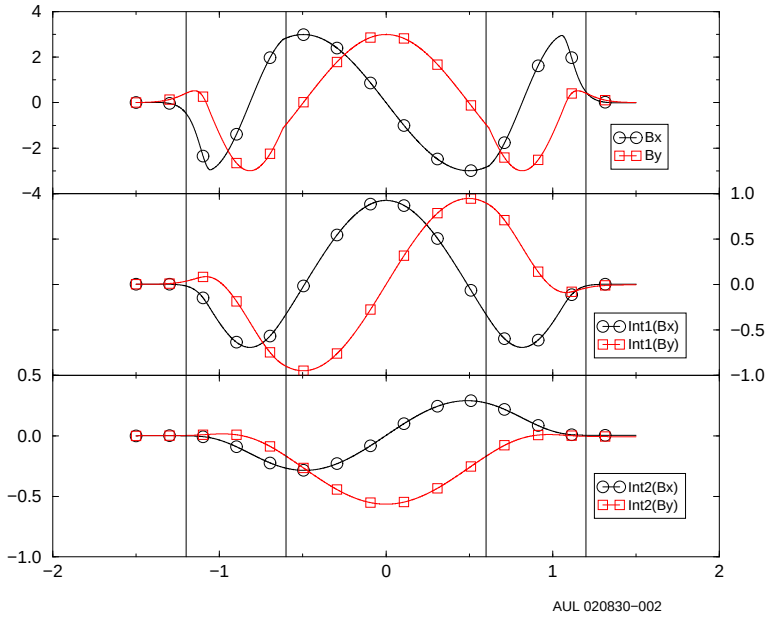


Figure 1: Field [T] and field integrals $[T-m]$ and $[T-m^2]$ on axis.Snake in three helices with: pitch-2, pitch-1, pitch-2. The boundaries of each helix is indicated by the vertical lines.

if $I_1^{(x)}(z_f) = 0$, it is $y'(z_f) = y'_0$.
if $y'_0 = 0$, and $I_2^{(x)}(z_f) = 0$, it is $y(z_f) = y_0$.

Fig. 1 shows the structure of the idealized snake magnetic field and of the field integrals. The snakes has 3 helices. The center helix has length $L_1$ and twist angle of $\Delta\theta_1$. The outer helices have length $L_2$ and twist angle $\Delta\theta_2$. All twists are in the same direction, say right-handed. From the top part of the figure it is apparent that the $x$ component of the field is an odd function of $z$, hence $I_1^{(x)}$ is even and $I_1^{(x)}(z_f) = 0$ in every case, for a perfectly symmetric snake. However, $B_y$ is even, then $I_1^{(y)}(z_f) \neq 0$ in general, unless we play with the pitches and the fringe field to make it vanish. If this happens, $I_1^{(y)}(z)$ is odd. From the bottom part of the figure we see that $I_2^{(x)}$ will not in general vanish because $I_1^{(x)}$ is even, and $I_2^{(y)}$ will not in general vanish because $I_1^{(y)}$ will be odd only if it is made to vanish.

In conclusion, only $I_1^{(x)}(z_f) = 0$ in general, which guarantees that the vertical angle of the beam is the same at the entrance and at the exit of the snake. In particular we can make $y'(z) = y'(0) = 0$, that is convenient because the AGS has limited vertical steering capabilities. We can adjust the other three integral to vanish using three parameters: the relative lengths of the inner and outer helices, with a total length kept fixed by the space constraint, and the two twist

Table 1: Parity of field and vanishing field integrals

| $B_x$ | $I_1^{(x)}$ | $I_2^{(x)}$ | $B_y$ | $I_1^{(y)}$ | $I_2^{(y)}$ |
|---|---|---|---|---|---|
| | $y' - y'_0$ | $y - y_0$ | | $x' - x'_0$ | $x - x_0$ |
| odd | even | odd | even | odd | even |

angles $\Delta\theta_1$ and $\Delta\theta_2$. When $I_1^{(y)}(z_f) = 0$ it is $x'(z) = x'(0)$. We can conveniently make this horizontal angle to vanish. Then we can make $I_2^{(x)}(z_f) = 0$ to makes $y(z) = y(0)$ and $I_2^{(y)}(z_f) = 0$ to make $x(z) = x(0)$.

From Eq.(3) we see that the $x$ or $y$ orbit have the same shape and parity as $I_2^{(y)}$ and $I_2^{(x)}$, respectively. $y$ (odd) is balanced, but $x$ (even) is not. It is convenient, using some horizontal steering in the AGS, to move the whole horizontal orbit sideways, to better use the space available inside the snake gap. That will appear more evident in the discussion and examples in the next sections.

The situation, for end-vanishing integrals is in Table 1

# 3 The Analytical Model

An analytical model of the field of an helix dipole makes use of the Blewett-Chasman [7] (BC) expression valid for an infinitely long structure. To second order in $x$ and $y$ it is

$$\begin{cases} b_x = -\sin\phi + \frac{1}{8}(3k^2x^2 + k^2y^2)\sin\phi - \frac{1}{4}k^2xy\cos\phi \\ b_y = \cos\phi - \frac{1}{8}(k^2x^2 + 3k^2y^2)\cos\phi + \frac{1}{4}k^2xy\sin\phi \\ b_z = ky\sin\phi + kx\cos\phi \end{cases} \tag{5}$$

with

$$\vec{B} = \frac{\mu I}{2\pi}\vec{b}, \quad \phi = k\,z, \quad k = \frac{2\pi}{\lambda}. \tag{6}$$

$I$ is the current in the coils and $\lambda$ the wavelength of the windings. The field of Eq.(5) satisfies Maxwell's equations to first order.

For helices of finite length, modeling the end field is difficult, in particular we were not able to find a close expression for the fringe field that would satisfy Maxwell's at the same time. So we will use an expression that fits at the best the field calculated by a numerical 3D code (like *Opera-3d*). The fringe field has the following properties (i) its amplitude falls off with distance in a characteristic length of one magnet gap; (ii) the rotation pitch of the field, expressed by $k$ in Eq.(6) decrease steadily from the last value reached at the end of the helix to a final value. A third problem in modeling the fringe field is that (iii) it is not immediate to define exactly when the fringe starts inside the helix. It is within a distance of the order of one gap from the physical ends of the windings and will be found by trial and error.

The three points above are very important, because, due to the near cancellation of the field integrals in a compensated snake, the role of the fringe field is essential. Approximately, many of the basic features of the snake can still be calculated using an hard edge model.

We built a snake model using the BC field and some first assumptions on the fringe fields. Then we used the code *Snig* [8] with this model, to track polarized particles through the field of the snake by integration of the equation for the orbit and the BMT Eq.(1) for the spin precession. In *Snig* the integration is performed by a Hamming Predictor Corrector 3.order algorithm with variable step size. The orbit equation is

$$\frac{d\vec{\beta}}{dt} = \vec{\beta} \times \vec{\Omega}, \quad \vec{\Omega} = \frac{e\vec{B}}{m\gamma}, \quad \beta^2 = 1 - \frac{1}{\gamma^2}, \quad \gamma = \frac{E}{m_0 c^2}, \tag{7}$$

with $E$ the total energy of the proton, and $m_0 c^2 = 0.938 GeV$ its rest energy. The position and angle of the orbit are calculated from

$$\begin{cases} x' = \frac{dx}{dz} = \frac{\beta_x}{\beta_z} \\ y' = \frac{dy}{dz} = \frac{\beta_y}{\beta_z} \end{cases}, \quad \beta_z = \frac{\beta}{\sqrt{1+x'^2+y'^2}} \quad \frac{dz}{dt} = \beta_z c \tag{8}$$

*Snig* calculates transfer maps through the snake for the $4 \times 4$ transverse orbit phase space and spin. For a first order orbit transfer, a set of eight extra particles with coordinates close to a leading particles are propagated and the transverse 4x4 orbit matrix is calcolated as the Jacobian

$$T_{ij} = \left( \frac{\partial x_i^{(f)}}{\partial x_j^{(0)}} \right), \tag{9}$$

where '0' and 'f' mean the beginning and the end of the trajectory. For higher order maps, more particles are required.

A spin rotation matrix through the snake is similarly calculated, by propagating three additional protons with the same orbit phase space coordinates, but slightly different spin values. The angle of spin precession through the snake and the orientation of the axis (two angles) can be calculated from the spin matrix [9].

*Snig* is also designed to track a test particle moving through a field described by a numerical map, like one generated by *Opera-3d*, with values of the field assigned to nodes of a 3D Cartesian mesh $(x, y, z)$. For the integration the code performs a 3-cubic interpolation on a cube of 27 mesh points. *Snig* has also provision to check the obeyance of the field to the Maxwell conditions

$$\vec{\nabla} \cdot \vec{B} = 0, \quad \vec{\nabla} \times \vec{B} = 0. \tag{10}$$

*Snig* can calculate field gradients and multipoles around a trajectory, by (a) sampling the field in points slightly off the orbit by $\delta x$, $\delta y$ and $\delta z$ and calculate numerically field derivatives by differences in three points, or (b) sampling the field on circles of small radius perpendicular to the $\vec{z}$ axis and centered on the

Table 2: Parameters for a Cold Snake model for the AGS

| Type | $B_0$ [T] | $\psi$ [deg] | $\theta$ [deg] | $z_c$ [m] | L [m] |
|---|---|---|---|---|---|
| Helix | 3. | -301.8 | 180. | 0.472 | 0.446 |
| Helix | 3. | -121.8 | 243.6 | 1.300 | 1.208 |
| Helix | 3. | 121.8 | 180. | 2.128 | 0.446 |

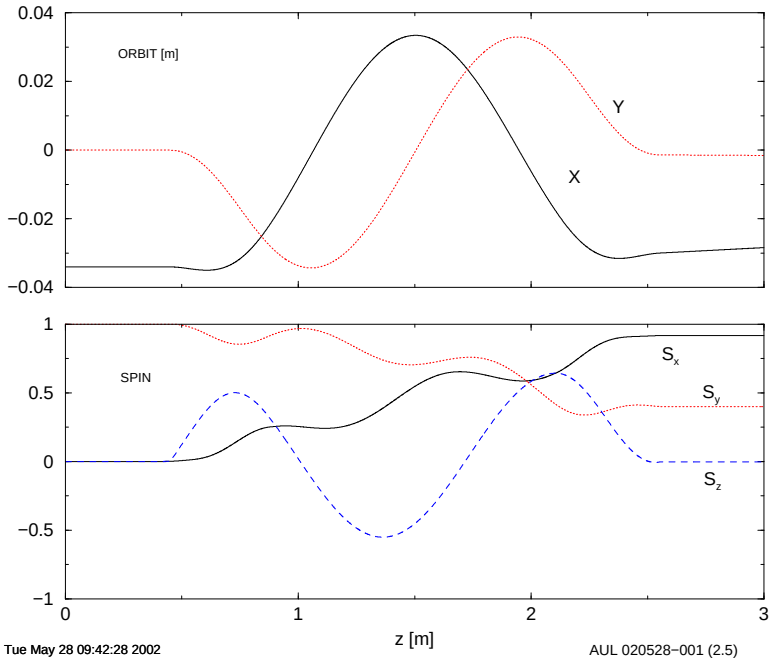


Figure 2: Orbit and spin for $\gamma = 2.5$. Model snake. *Snig* tracking

orbit and perform an FFT on the data, to find both amplitude and phase of the multipoles. Examples will be shown later in this note.

A starting list of parameters for the model is in Table 2. The field is the one shown in Fig. 1. Tracking results for orbit and spin for three proton energies in the AGS, between injection and extraction are shown in Figs. 2,3,4. The figures show the orbit and the spin evolution of the components in the snake. The spin is taken with its orientation up along $y$, vertical, at snake entrance. We see that (i) the orbit maximum excursion decreases with increasing energy, so, the orbit may cause problems at injection; (ii) the spin rotation decreases somewhat with increasing energy.

Numerical values for these energy values of $\gamma = 2.5, 15$ and 26 found by integration with *Snig* are summarized (orbits) in tables 3, 4, 5 Spin rotation angles and matrices for the same energies are in tables 6, 7, 8.

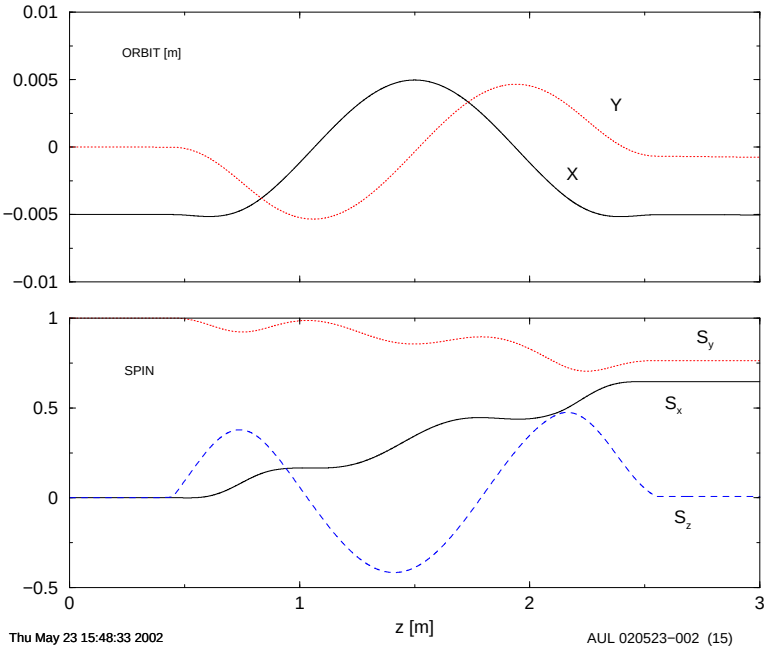


Figure 3: Orbit and spin for $\gamma = 15$. Model snake. *Snig* tracking

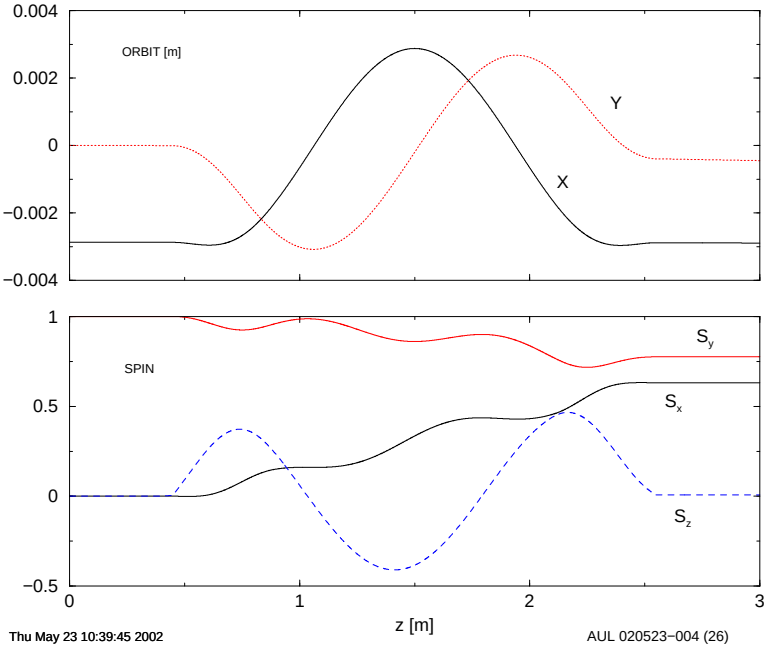


Figure 4: Orbit and spin for $\gamma = 26$. Model snake. *Snig* tracking

Table 3: Model Snake. *Snig* Tracking. Orbit. $\gamma = 2.5$

| | | | |
|---|---|---|---|
| Field integrals (x,y,z) [T-m] | 4.355 | 3.721 | 0.246 |
| Traj Lengthening [mm] | 11.888 | | |
| Max excursion x,y [mm] | 34.965 | 34.290 | |
| Matrix | | | |
| 0.30719700E+00 | 0.21801306E+01 | -0.17216739E+00 | -0.13550548E+00 |
| -0.41081700E+00 | 0.35019913E+00 | -0.49240775E-01 | -0.20082603E-01 |
| -0.17622600E+00 | -0.13007265E+00 | 0.89416433E+00 | 0.27031945E+01 |
| -0.63495000E-01 | -0.28623115E-01 | -0.16502073E+00 | 0.62307528E+00 |
| det = 1.00000000 | | | |

Table 4: Model Snake. *Snig* Orbit. $\gamma = 15$

| | | | |
|---|---|---|---|
| Field integrals (x,y,z) [T-m] | 4.331 | 3.667 | 0.638 |
| Traj Lengthening [mm] | 0.2733858 | | |
| Max excursion x,y [mm] | 5.152 | 5.334 | |
| Matrix | | | |
| 0.98066800E+00 | 0.29820880E+01 | -0.94783113E-02 | 0.66580959E-02 |
| -0.15631000E-01 | 0.97199884E+00 | -0.11242272E-01 | -0.10968952E-01 |
| -0.22972000E-01 | -0.34007460E-01 | 0.99843342E+00 | 0.30075856E+01 |
| -0.11189000E-01 | -0.24348282E-01 | -0.70541160E-04 | 0.10011774E+01 |

Table 5: Model Snake. *Snig* Orbit. $\gamma = 26$

| | | | |
|---|---|---|---|
| Field integrals (x,y,z) [T-m] | 4.331 | 3.666 | 0.689 |
| Traj Lengthening [mm] | 0.091 | | |
| Max excursion x,y [mm] | 2.961 | 3.078 | |
| Matrix | | | |
| 0.99263300E+00 | 0.29975260E+01 | -0.46262441E-02 | 0.51200503E-02 |
| -0.77690000E-02 | 0.98389851E+00 | -0.64039727E-02 | -0.63336283E-02 |
| -0.13008000E-01 | -0.20083071E-01 | 0.10002895E+01 | 0.30121988E+01 |
| -0.64230000E-02 | -0.14689663E-01 | 0.24695103E-02 | 0.10070850E+01 |
| det = 1.00000000 | | | |

Table 6: Model Snake. *Snig* Spin precession. $\gamma = 2.5$

| | | |
|---|---|---|
| Spin matrix | | |
| 0.91646067 | 0.39962872 | 0.01991794 |
| 0.43620606 | -1.09093197 | -0.01196463 |
| -0.01849256 | 0.00327697 | 1.00020379 |
| Precession: | $\mu$ = 66.447 deg | |
| Axis: | $\phi$ = 179.035 deg | $\theta$ = -0.427 deg |

Table 7: Model Snake. *Snig* Spin precession. $\gamma = 15$

| Spin matrix | | |
|---|---|---|
| 0.76327577 | 0.64606521 | -0.00313690 |
| -0.84640036 | 1.31000294 | -0.01690750 |
| -0.00892731 | 0.01425395 | 1.00010650 |
| Precession: | $\mu$ = 38.036 deg | |
| Axis: | $\phi$ = -0.071 deg | $\theta$ = -0.149 deg |

Table 8: Model Snake. *Snig* Spin precession. $\gamma = 26$

| Spin matrix | | |
|---|---|---|
| 0.77556503 | 0.63126066 | -0.00297816 |
| -0.81390355 | 1.28925379 | -0.01623770 |
| -0.00826574 | 0.01381515 | 1.00009986 |
| Precession: | $\mu$ = 39.153 deg | |
| Axis: | $\phi$ = -1.198 deg | $\theta$ = -0.156 deg |

# 4 Fitting Field maps

The pure analytical model of the snake as described in sec. 3 gives a good feeling that a snake with the proposed structure would work. The next step was to model the snake with the 3D code *Opera-3d* that calculates the field produced by a set of current carrying coils. This work was carried on in parallel at the Magnet Division of Brookhaven (BNL-MD) and at the Riken Institute in Tokyo. Details are reported elsewhere [5], [6].

In this section we will describe how the analytical model was used to optimize the snake structure, and how the results were fed back to the Magnet Division to arrive at a final design of the cold snake. A similar approach was used for the warm snake and will be described in a further note.

The process of fitting was developed in four phases, with iterations

• The Magnet Division creates a numerical field map on a 3D mesh with *Opera3D* on the basis of a preliminary design;

• We identify the key features of the snake to be parametrized in the model;

• Run *Snig* using the model fitted according to the map in an optimization loop. Clearly, running *Snig* on the model takes only a small fraction of the time than writing the input and run *Opera3D*;

• Translate the computer results into useful parameters for the map makers in the Magnet Division, so they can create a new map;

• Iterate the last two steps until a satisfactory result for the basic design is reached;

• As a final touch, aim to further refinements like corrections of coupling, focusing, multipoles etc.

For the fitting of the model to the map, in addition to the three basic fitting

Table 9: No. of parameters for fitting

| loop parameters | | auxiliary parameters | | |
|---|---|---|---|---|
| length ratio | twist of helices | field ampl | tail fall-off | asympt. value of |
| $L_1/L_2$ | $\Delta\theta_{1,2}$ | of $B$ | pitch | pitch $\Delta\theta_e$ |
| 1 | 2 | 3 | 3 | 1 |

parameters already described, namely the relative length and twist angles of the helices, we needed extra parameters for fitting curves for (i) the maximum intensity of the field along the helix, and (ii) the field fall-off at magnet ends, both in amplitude and in angle. Fitting was done with quadratic functions with three parameters each. (iii) Finally, we needed an extra parameter representing the asymptotic value of the field angle away from the magnet at both ends. Finally we had 3 basic + 10 auxiliary parameters to vary, as shown in Table 9 However, it was expected that only the 3 "basic" had to be used in the iterative process (loop), because the coefficients of the cubic fitting curve and the asymptotic angles could be determined once for all at the beginning of the exercise, since they are mostly related to the structure of the magnet end regions. All ten parameters are in the input of *Snig*.

The field angle or running pitch is the basic quantity to describe the snake field (the spinal cord of the model)

$$\phi = -\arctan\frac{B_x}{B_y}. \tag{11}$$

This angle coincides with the angle defined in Eq.(6), when evaluated on the snake axis. The field angle fall-off can be determined from the map. A $\phi$ curve derived from one of the maps provided by the Magnet Division, on axis, is shown in Fig. 5. The figure clearly shows the higher pitch of helices 1 and 3, as compared with the pitch of helix 2 (less slope). The quadratic fitting of $\phi$ at both ends and in the transition region with its asymptotic value and between helices is in the plot.

The first step of fitting was to determine a starting set of parameters for the pitch curve $\phi$ and for the field amplitude in the helices. Then, we proceeded to vary the three basic structural parameters: length ratio and twist angles, in order to obtain a compensation of the field integrals. Work charts for optimization loops are graphically shown in Fig. 6 and 7.

It took three steps to arrive at a satisfactory solution. Based on the first analytical model of the snake a first numerical *Opera3D* map was created by R.Gupta et al of the Magnet Division. Fitting of this map and loop optimization with the model generated a new set of parameters. A second numerical map was created. To this improved map a solenoid was added to correct for coupling and the model was used again to optimize the new map including the solenoid. The final, optimized, fit is in Fig. 8 that shows the transverse components of the numerical field on axis compared with the model field. The boundaries of

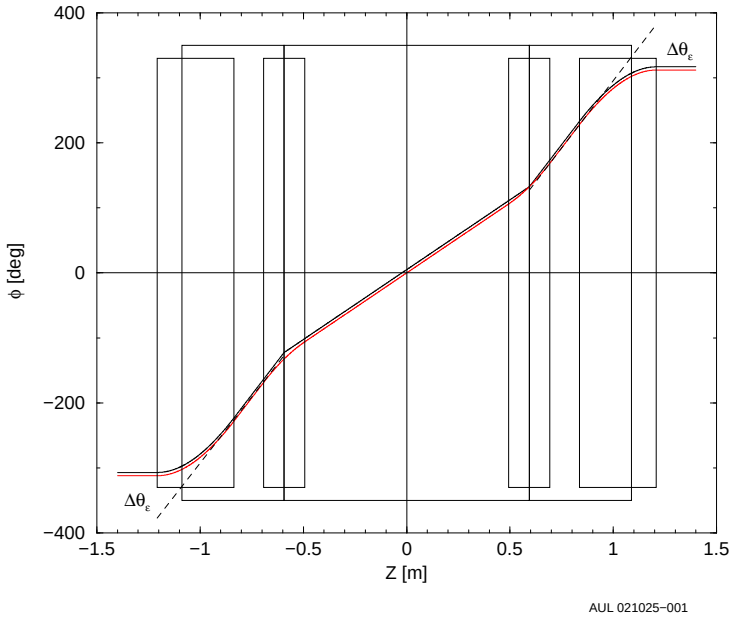


Figure 5: Fitting of a map with a model. Pitch angle $\phi$. We also show the boundaries of the individual helices and of the fringe regions and the end value of the pitch angle $\Delta\theta_e$. From R.Gupta map v4-x06.

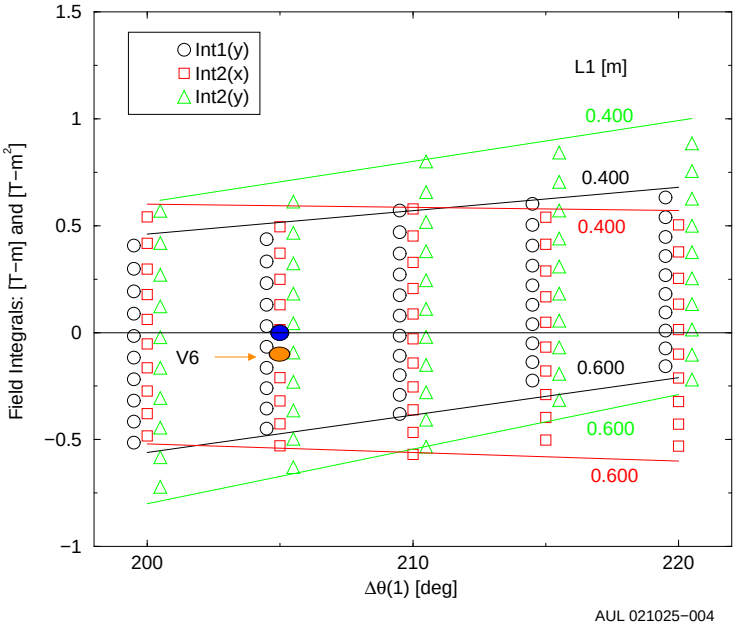


Figure 6: Optimization loop for Map x6-v06. Fixed $\Delta\theta_2 = 255deg$, vary $L_1$ and $\Delta\theta_1$. A full dot represents the starting and the final working point.

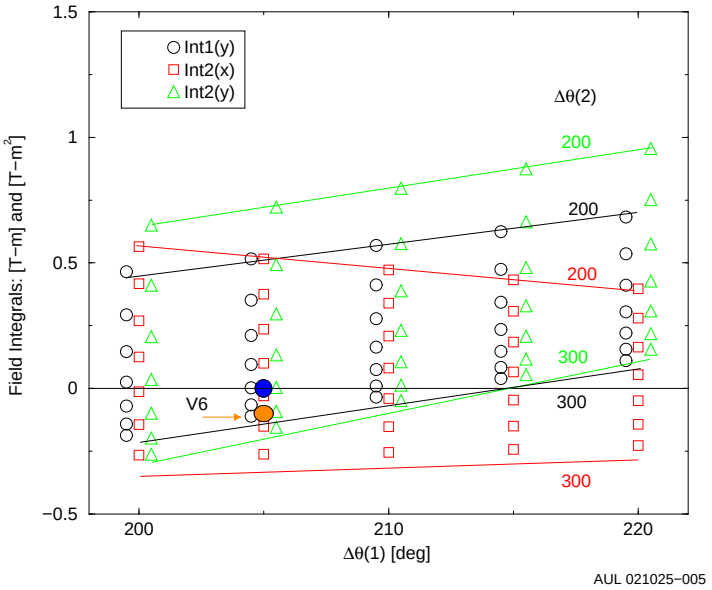


Figure 7: Optimization loop for Map x6-v06. Fixed lengths: 0.495 and 1.1862 $m$, vary $\Delta\theta_1$ and $\Delta\theta_2$. A full dot represents the starting and the final working point.

the three helices are shown, and also the pitch angle function $\phi$.

The parameters of this optimized design of the snake are given in Table 10. Here, $\Delta\theta$ is the full rotation of the field in each helix, the full length of the device excluding the fringe extension is 2.1762 $m$, and the fringe is seen from the model-matched map to extend 25.4 $mm$ inward and 12 $mm$ outward, i.e. this is the distance of the field fall-off. The full bore of the device, to the inner surface of the coils is 100 $mm$. This map contains also a solenoid to compensate for coupling, that will be discussed in a later section.

The field and field integrals on axis for this optimized configuration are

Table 10: Parameters for a snake designed with *Opera3D* after optimization with *Snig*. Map v4.3-x06+sol5 (Gupta)

| Type | $B_0$ [T] | $\Delta\theta_e$ [deg] | L [m] | fringe in/out [mm] |
|---|---|---|---|---|
| Helix | 2.8480 | 205 | 0.4950 | 25.24 / 12.00 |
| Helix | 3.1197 | 255 | 1.1862 | |
| Helix | 2.8480 | 205 | 0.4950 | |
| Solenoid | 0.2 | | 1.0 | |

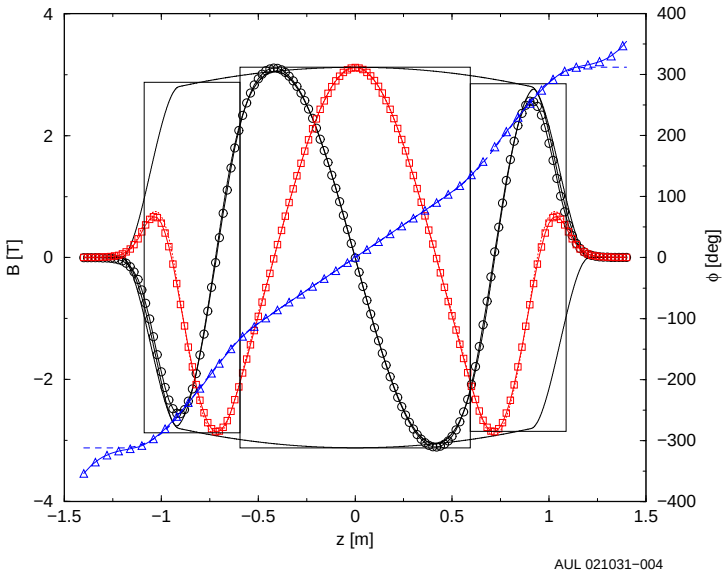


Figure 8: Model on Axis (symbol curves) compared with Gupta *Opera-3d* map v4.3-x06 (solid lines)

shown in Fig.9. The final values of the integrals are

$$\begin{array}{llll} I_1^{(x)} = & 0.0116724[T-m], & I_1^{(y)} = & 0.05588558[T-m] \\ I_2^{(x)} = & -0.100355,[T-m^2] & I_2^{(y)} = & 0.07559[T-m^2] \end{array}$$

# 5 Coupling and focusing

Off axis, a substantial longitudinal field $B_z$ is present, that would show up on any orbit (Fig. 10, for proton energy $\gamma = 2.5$), that can be compensated with a solenoid. This field is zero on axis, according to the third of Eqs.(5). The longitudinal field produces coupling between the $x$ and $y$ motion and is undesirable. From the transfer matrix for the snake it appeared also that the snake possesses a substantial amount of focusing in both planes. Coupling and focusing will distort the AGS lattice.

To characterize transverse coupling and focusing, refer to the first order transfer map for the snake.

$$R = \begin{pmatrix} |x,x| & |x,x'| & |x,y| & |x,y'| \\ |x',x| & |x',x'| & |x',y| & |x',y'| \\ |y,x| & |y,x'| & |y,y| & |y,y'| \\ |y',x| & |y',x'| & |y',y| & |y',y'| \end{pmatrix}, \tag{12}$$

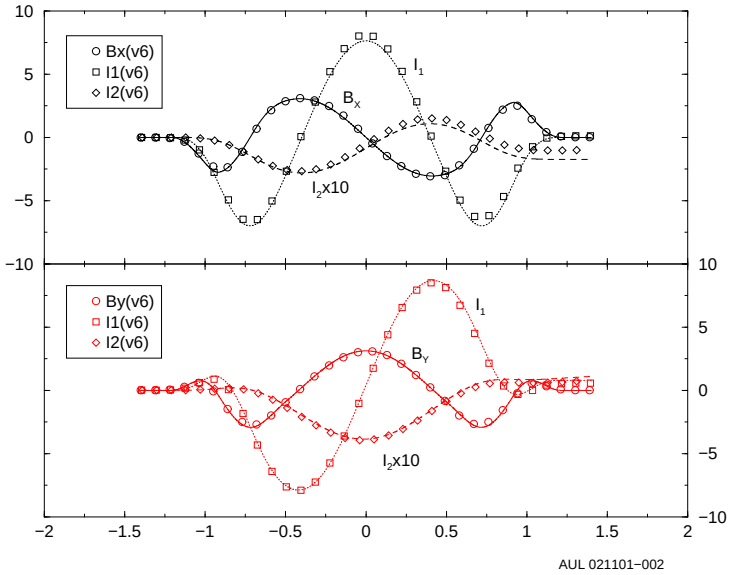


Figure 9: Field $[T]$ and field integrals $[T-m]$ and $[T-m^2]\times 10$ on axis for Gupta Map V4-X06, after optimization with Model 6. Upper plots: $B_x$, $I_1^{(x)}$, $I_2^{(x)}$. Lower plots, same for $y$.

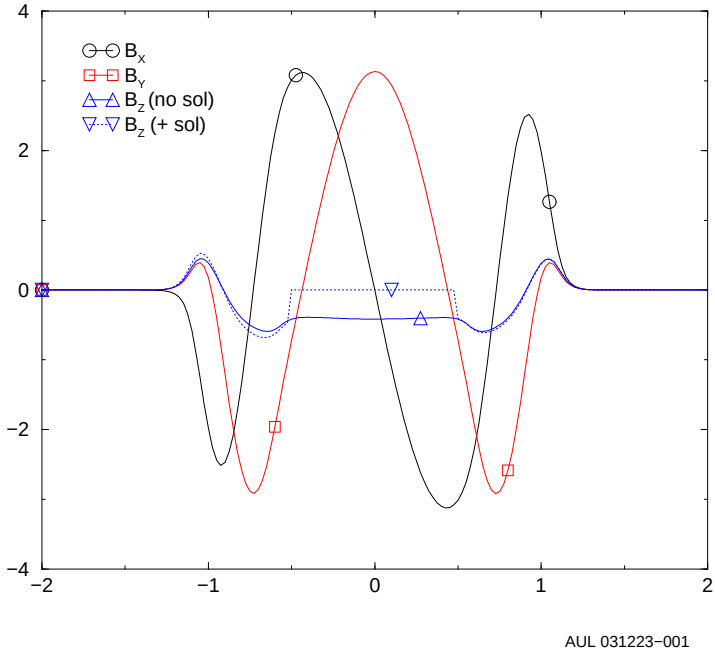


Figure 10: Field components on orbit for Gupta Map V4-X06, with and without a solenoid (not optimized). Energy $\gamma = 2.5$.

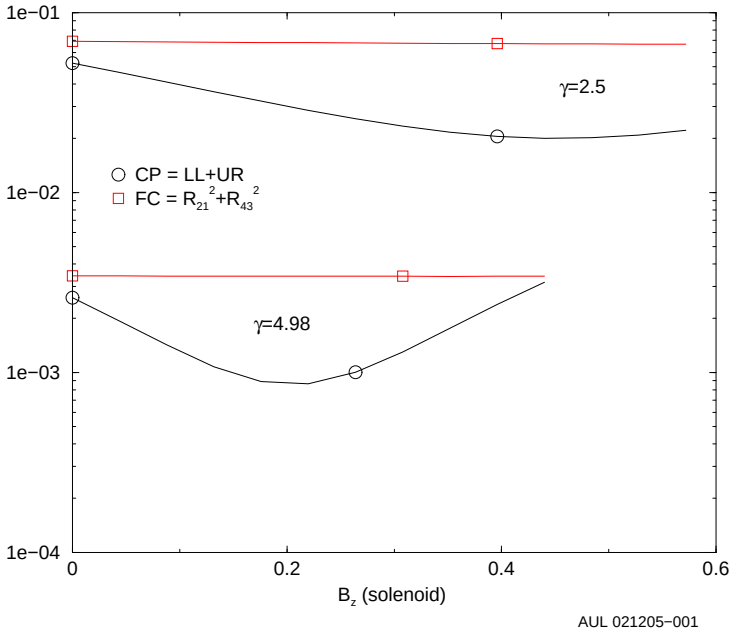


Figure 11: Snake map v4-x06 (Gupta) with added solenoid. Coupling and focusing as a function of solenoid strength at two beam energies: $\gamma = 2.5$ (injection) and $\gamma = 4.98$ (first depolarizing resonance in the AGS).

and define the following parameters

$$\begin{cases} LL = |y,x|^2 + |y,x'|^2 + |y',x|^2 + |y',x'|^2 \\ UR = |x,y|^2 + |x,y'|^2 + |x',y|^2 + |x',y'|^2 \\ CP = LL + UR \\ FC = |x',x|^2 + |y',y|^2 \end{cases} . \tag{13}$$

$CP \approx 0$ means no coupling and, and $FC \approx 0$ means no focusing.

The most direct solution to correct coupling is to add a solenoid in the middle of the snake that would cancel the longitudinal snake field component (as suggested by W.W.MacKay). Accordingly, the Magnet Division added a 1 m long solenoid to their maps. Following the procedure of model fitting and optimization described above, we searched for the optimum solenoidal field that would minimize coupling. Fig. 11 shows coupling and focusing as a function of solenoid strength. The figure shows that the best solenoidal field to minimize coupling is 0.2 $T$, and also that the solenoid has almost no effect on focusing, as expected. Fig. 12 shows transfer matrix elements as a function of solenoid strength. Correcting focusing in both planes is a much more difficult task than correcting coupling. It can be accomplished in principle but that may be prove impossible in practice whitout using elements external to the snake, because of lack of space to insert innside the snake additional correcting magnets.

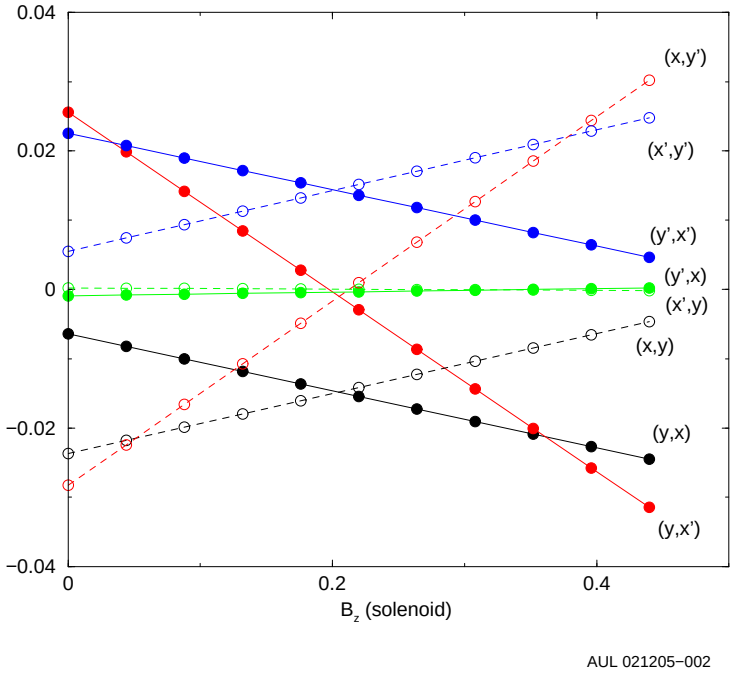


Figure 12: Snake map v4-x06 (Gupta) with added solenoid. Coupling matrix elements as a function of solenoid strength at beam energy $\gamma = 4.98$ (first depolarizing resonance).

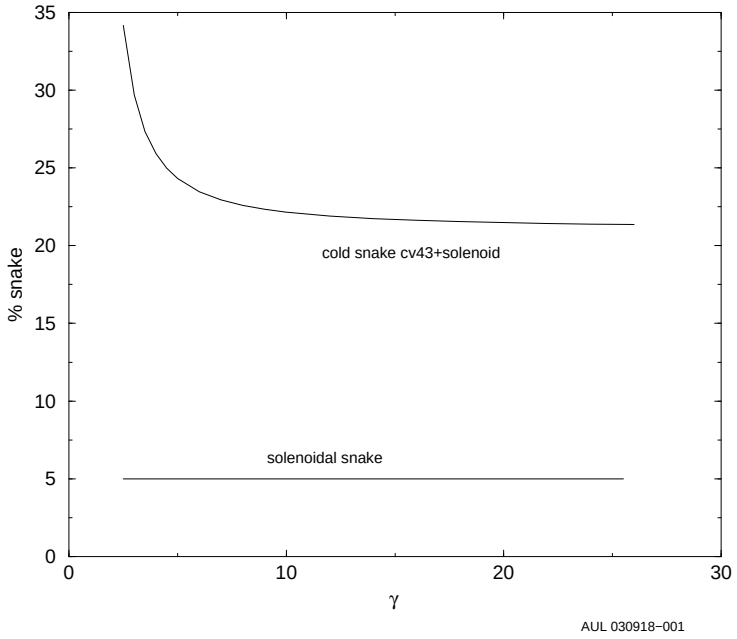


Figure 13: Spin rotation produced by snake v4_3-x06+sol5, vs. proton energy

Before discussing possible strategies, we will show the result of *Snig* tracking on the snake up to the point of solenoid correction. The snake field is described by the *Opera-3d* numerical map 'v4_3-x06+sol5' prepared by the Magnet Division.

# 6 Figures and Tables for the final cold snake

Figures 13,14,15 show the performance as spin rotator, coupling and focusing - see Eq(13)- of the final design as compared with the existing AGS solenoid snake. Coupling and focusing decrease wih energy. Figures 16, 17 show the orbit at various energy Field, Trajectories, Spin and matrices are shown in detail the following figures 18,19,20,22,23, and tables 11,12,13 for different proton energies in the AGS. The figures are similar to the ones obtained with the model, namely Figures 2,3,4.

Orbit matrice $R$ proved well symplectic, as we checked by verifying how well the condition was met

$$R^T S R - S = 0, \tag{14}$$

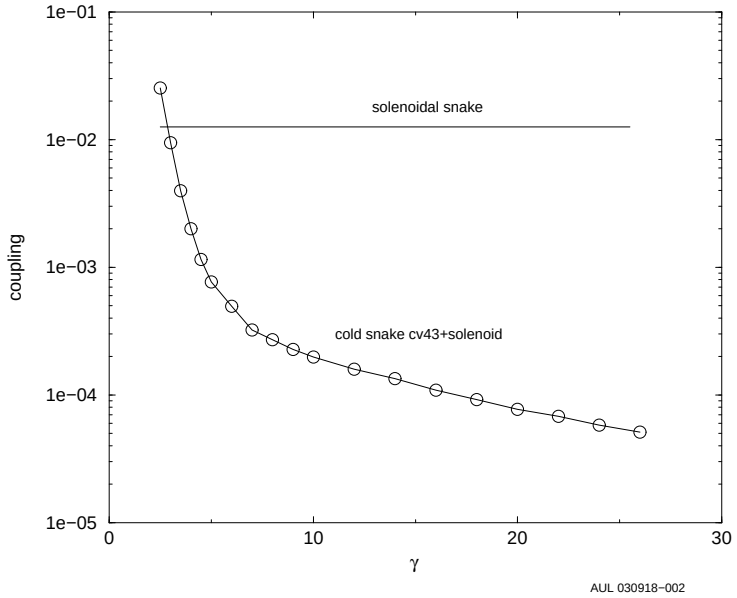


Figure 14: Coupling induced by snake v4_3-x06+sol5, vs. proton energy

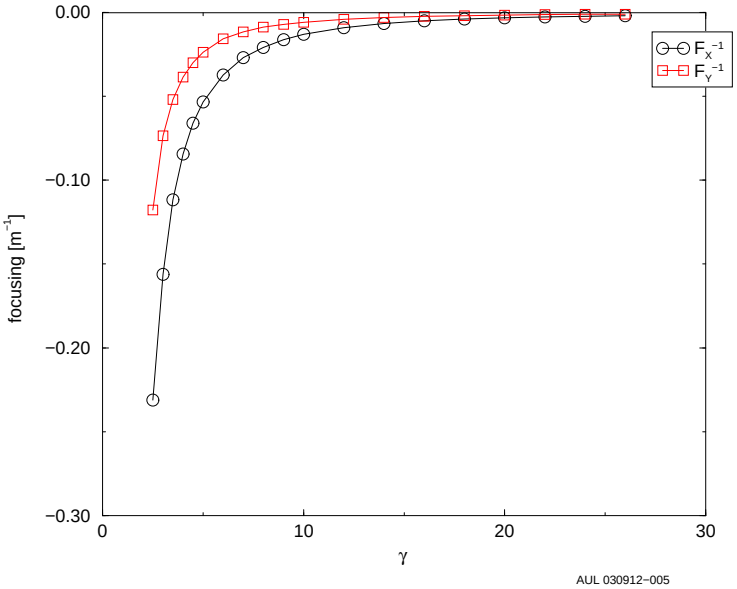


Figure 15: Focusing induced by snake v4_3-x06+sol5, vs. proton energy. The snakes is focusing in both planes

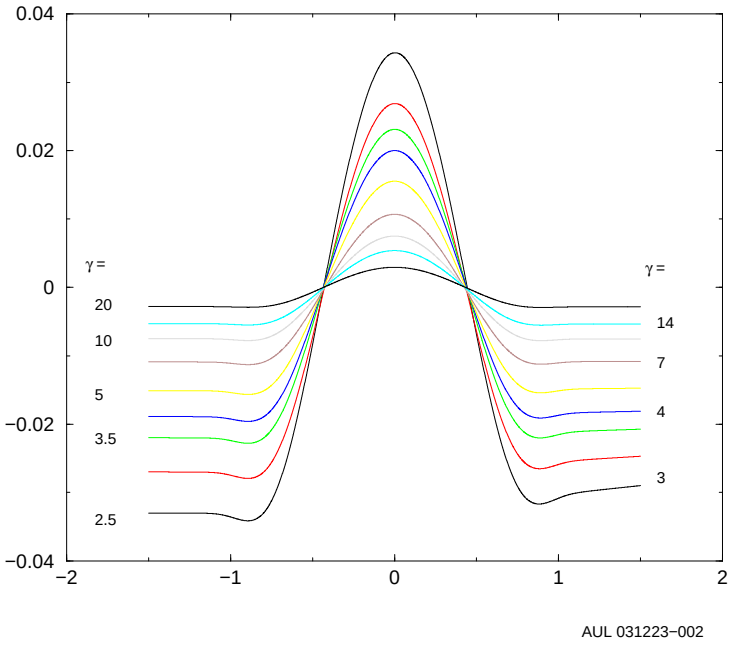


Figure 16: Horizontal orbit of snake v4_3-x06+sol5, vs. proton energy.

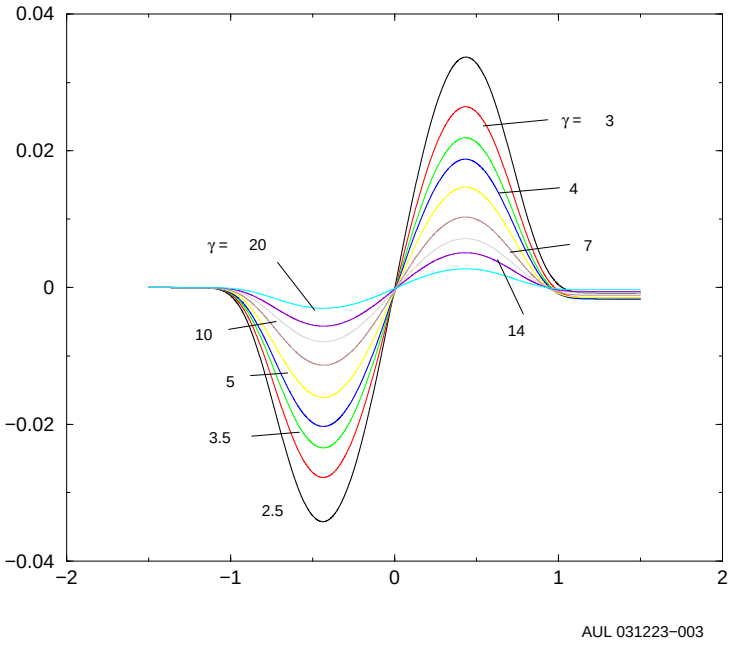


Figure 17: Verticalontal orbit of snake v4_3-x06+sol5, vs. proton energy.

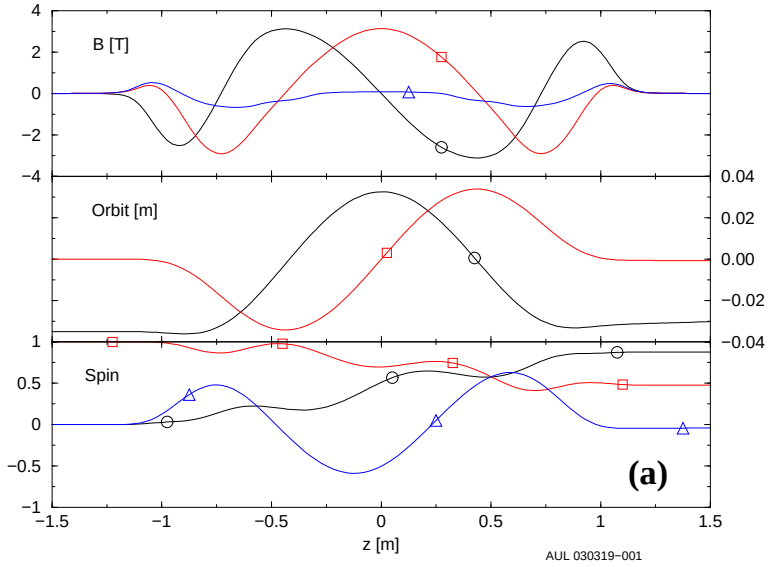


Figure 18: Field, orbit and spin for map v4_3-x06+sol5 (Gupta) for $\gamma = 2.5$. Circle: $x-$quantities, box: $y-$quantities, triangle: $z-$quantities.

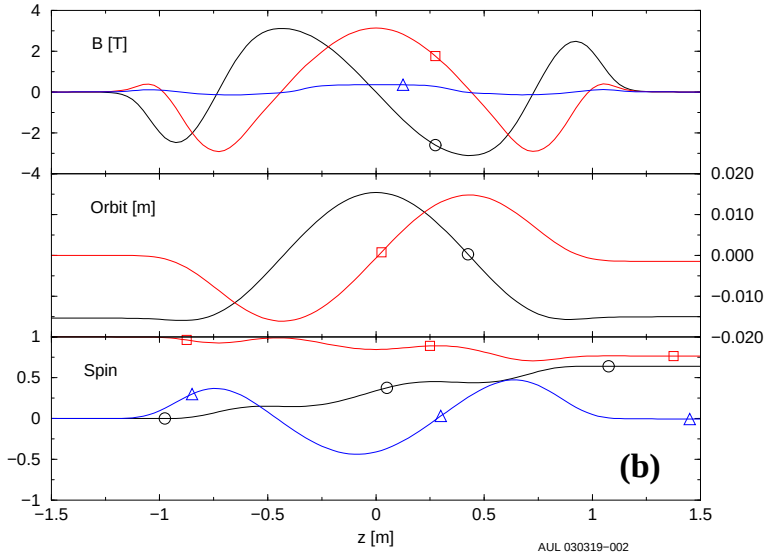


Figure 19: Field, orbit and spin for map v4_3-x06+sol5 (Gupta) for $\gamma = 4.98$. Circle: $x-$quantities, box: $y-$quantities, triangle: $z-$quantities.

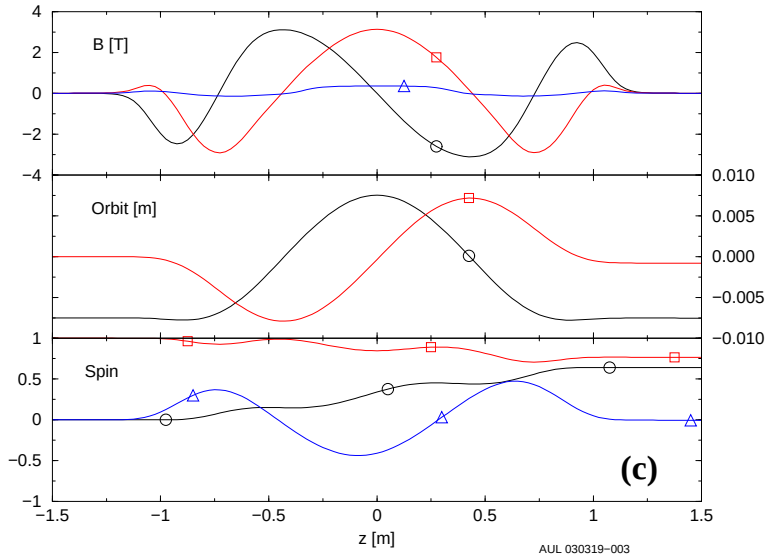


Figure 20: Field, orbit and spin for map v4_3-x06+sol5 (Gupta) for $\gamma = 10$. Circle: $x-$quantities, box: $y-$quantities, triangle: $z-$quantities.

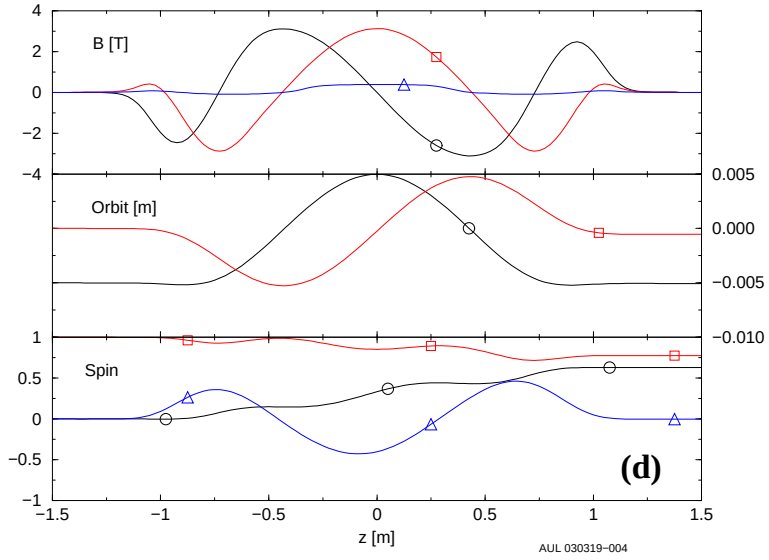


Figure 21: Field, orbit and spin for map v4_3-x06+sol5 (Gupta) for $\gamma = 15$. Circle: $x-$quantities, box: $y-$quantities, triangle: $z-$quantities.

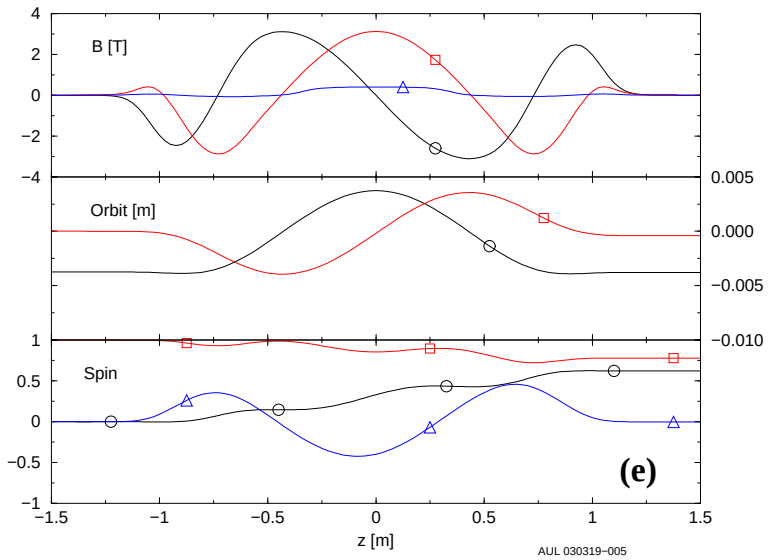


Figure 22: Field, orbit and spin for map v4_3-x06+sol5 (Gupta) for $\gamma = 20$. Circle: $x-$quantities, box: $y-$quantities, triangle: $z-$quantities.

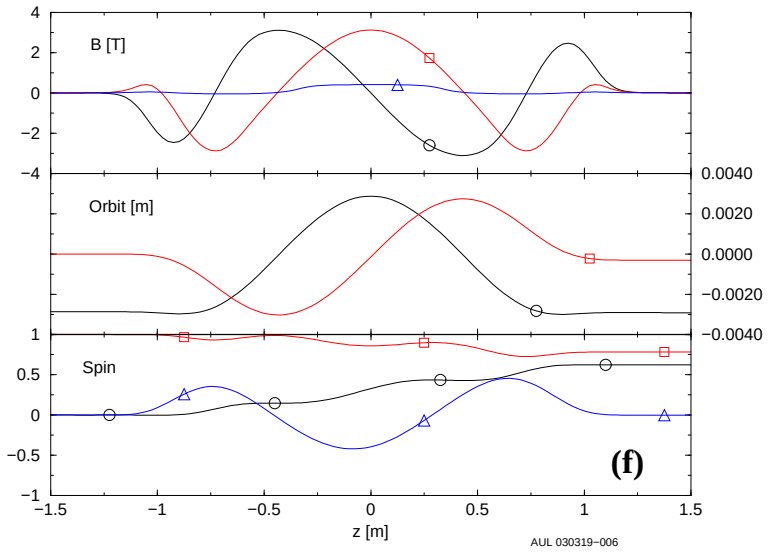


Figure 23: Field, orbit and spin for map v4_3-x06+sol5 (Gupta) for $\gamma = 26$. Circle: $x-$quantities, box: $y-$quantities, triangle: $z-$quantities.

Table 11: Map v4_3-x06+sol5 (Gupta).
*Snig* tracking results. Spin

| Energy | Precess.angle | Axis angles | |
|---|---|---|---|
| $\gamma$ | $\mu$ [deg] | $\phi$ [deg] | $\theta$ [deg] |
| 2.5 | 61.5085798 | -180.0000000 | 0.0000275 |
| 3. | 53.4464552 | -179.9999998 | 0.0000192 |
| 4. | 46.6467221 | -179.9999999 | 0.0000177 |
| 5. | 43.7779582 | 180.0000000 | 0.0000170 |
| 7. | 41.2989797 | 179.9999997 | 0.0000144 |
| 10. | 39.8924228 | 179.9999996 | 0.0000109 |
| 14. | 39.1425935 | 179.9999996 | 0.0000084 |
| 20. | 38.6712667 | 179.9999996 | 0.0000064 |
| 26. | 38.4464882 | 179.9999996 | 0.0000053 |

Table 12: Map v4_3-x06+sol5 (Gupta).
*Snig* tracking results. Orbit

| Energy | Max excursion | | Coupling | Focusing | | Orb. lengthening |
|---|---|---|---|---|---|---|
| $\gamma$ | $x$ [mm] | $y$ [mm] | | in $x$ [$m^{-1}$] | in $y$ [$m^{-1}$] | $\delta$L [mm] |
| 2.5 | 34.3305192 | 34.2494635 | 0.025329 | -0.231141 | -0.117786 | 12.0586674 |
| 3. | 27.9422948 | 27.7869174 | 0.009446 | -0.156236 | -0.073526 | 7.8022010 |
| 4. | 20.0202768 | 20.3213702 | 0.002000 | -0.084332 | -0.038537 | 4.1161719 |
| 5. | 15.6539064 | 16.0730290 | 0.000767 | -0.053362 | -0.023624 | 2.5623310 |
| 7. | 11.2929001 | 11.3699445 | 0.000323 | -0.026955 | -0.011605 | 1.2778029 |
| 10. | 7.7873180 | 7.9189642 | 0.000198 | -0.012992 | -0.005725 | 0.6190552 |
| 14. | 5.5250811 | 5.6431593 | 0.000134 | -0.006535 | -0.002910 | 0.3142885 |
| 20. | 3.9662490 | 3.9453283 | 0.000077 | -0.003172 | -0.001479 | 0.1536416 |
| 26. | 2.9420576 | 3.0334369 | 0.000051 | -0.001824 | -0.000925 | 0.0908394 |

Table 13: Map v4_3-x06+sol5 (Gupta). Orbit trasfer maps.

| | | | | |
|---|---|---|---|---|
| $\gamma = 2.5$ | 0.634363 | 2.587046 | -0.088141 | -0.068172 |
| det = 1.00001808 | -0.231141 | 0.639455 | 0.003130 | 0.042579 |
| | -0.059485 | 0.048541 | 0.827929 | 2.735008 |
| | -0.013834 | 0.070741 | -0.117786 | 0.822990 |
| $\gamma = 3.0$ | 0.757050 | 2.728119 | -0.054622 | -0.034768 |
| det = 0.999999 | -0.156236 | 0.760087 | 0.000826 | 0.031024 |
| | -0.038252 | 0.024816 | 0.892216 | 2.832637 |
| | -0.005728 | 0.046674 | -0.073526 | 0.889223 |
| $\gamma = 3.5$ | 0.828188 | 2.807805 | -0.035215 | -0.017680 |
| det = 1.000001 | -0.111747 | 0.829584 | 0.000271 | 0.023431 |
| | -0.026579 | 0.012150 | 0.923339 | 2.882509 |
| | -0.002490 | 0.031662 | -0.051875 | 0.921965 |
| $\gamma = 4.0$ | 0.871275 | 2.856106 | -0.024411 | -0.008111 |
| det = 1.000001 | -0.084332 | 0.871831 | 0.000113 | 0.019187 |
| | -0.020757 | 0.004625 | 0.942714 | 2.912987 |
| | -0.001211 | 0.022723 | -0.038537 | 0.942183 |
| $\gamma = 5.0$ | 0.919316 | 2.909965 | -0.013253 | 0.001191 |
| det = 1. | -0.053362 | 0.919059 | 0.000037 | 0.014339 |
| | -0.014572 | -0.002904 | 0.964540 | 2.946946 |
| | -0.000281 | 0.012794 | -0.023624 | 0.964781 |
| $\gamma = 7.0$ | 0.959696 | 2.955185 | -0.004677 | 0.006777 |
| det = 0.999996 | -0.026955 | 0.959039 | 0.000062 | 0.009539 |
| | -0.009300 | -0.007406 | 0.982285 | 2.974416 |
| | 0.000048 | 0.004787 | -0.011605 | 0.982939 |
| $\gamma = 10$ | 0.980803 | 2.978896 | -0.000733 | 0.007745 |
| det = 1.000002 | -0.012992 | 0.980120 | 0.000090 | 0.006221 |
| | -0.005922 | -0.007909 | 0.991070 | 2.988171 |
| | 0.000111 | 0.001035 | -0.005725 | 0.991756 |
| $\gamma = 16$ | 0.992810 | 2.992299 | 0.000865 | 0.006432 |
| det = 0.999994 | -0.004963 | 0.992282 | 0.000081 | 0.003666 |
| | -0.003412 | -0.006417 | 0.996267 | 2.996028 |
| | 0.000092 | -0.000605 | -0.002312 | 0.996786 |
| $\gamma = 20$ | 0.995462 | 2.995383 | 0.001013 | 0.005559 |
| det = 1. | -0.003172 | 0.995013 | 0.000071 | 0.002665 |
| | -0.002684 | -0.005526 | 0.997557 | 2.997895 |
| | 0.000077 | -0.000790 | -0.001479 | 0.998073 |
| $\gamma = 26$ | 0.997443 | 2.997688 | 0.001045 | 0.004578 |
| -det = 1.000055 | 0.001824 | 0.997080 | 0.000060 | 0.001993 |
| | -0.001994 | -0.004527 | 0.998431 | 2.999156 |
| | 0.000063 | -0.000859 | -0.000925 | 0.998844 |

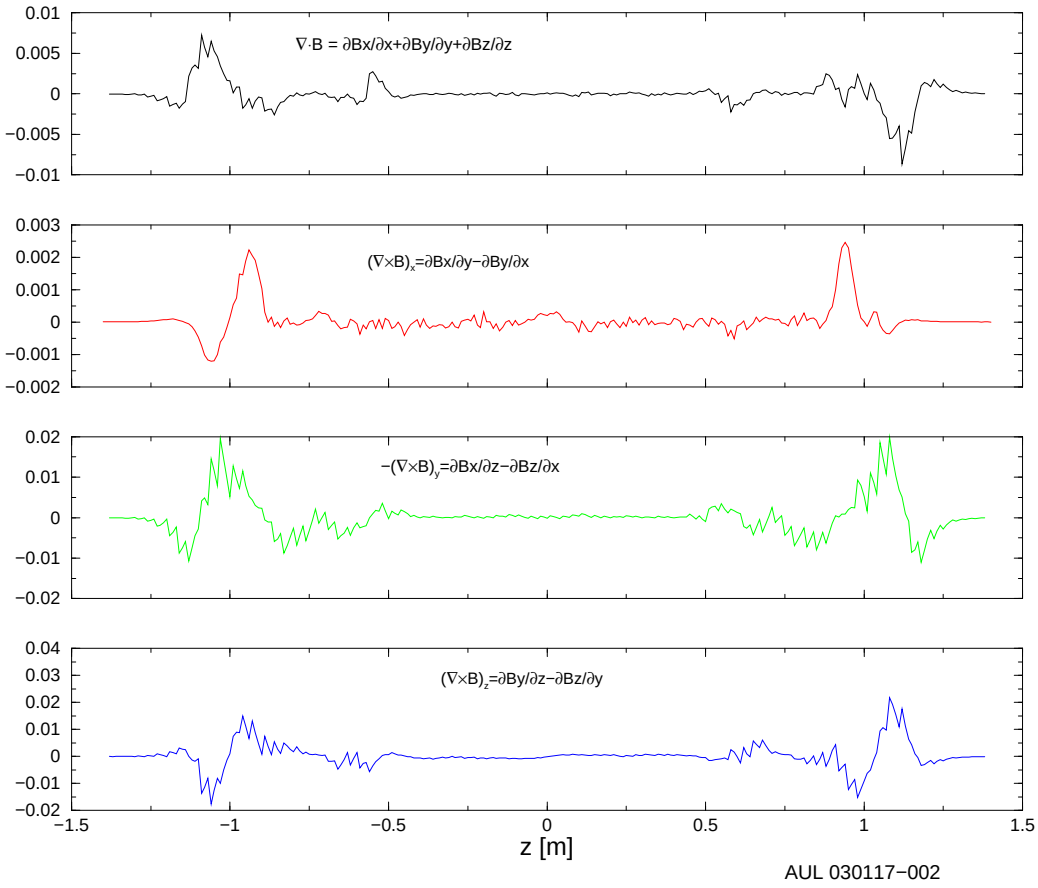


Figure 24: Div and Components of Curl of B along the $\gamma = 4.98$ trajectory

where $R^T$ is the transpose of $R$, and $S$ is the matrix

$$S = \begin{pmatrix} 0 & 1 & 0 & 0 \\ -1 & 0 & 0 & 0 \\ 0 & 0 & 0 & 1 \\ 0 & 0 & -1 & 0 \end{pmatrix}. \tag{15}$$

Symplecticity also means that the map field obeys Maxwell Equations (10). Div and Curl conditions along a trajectory through the map are shown in Fig. 24

# 7 Multipoles. Attempts at correcting focusing and gradients

To investigate the content of multipoles in the snake field, we calculate the field components in 128 points along a circle centered on axis in a vertical plane,

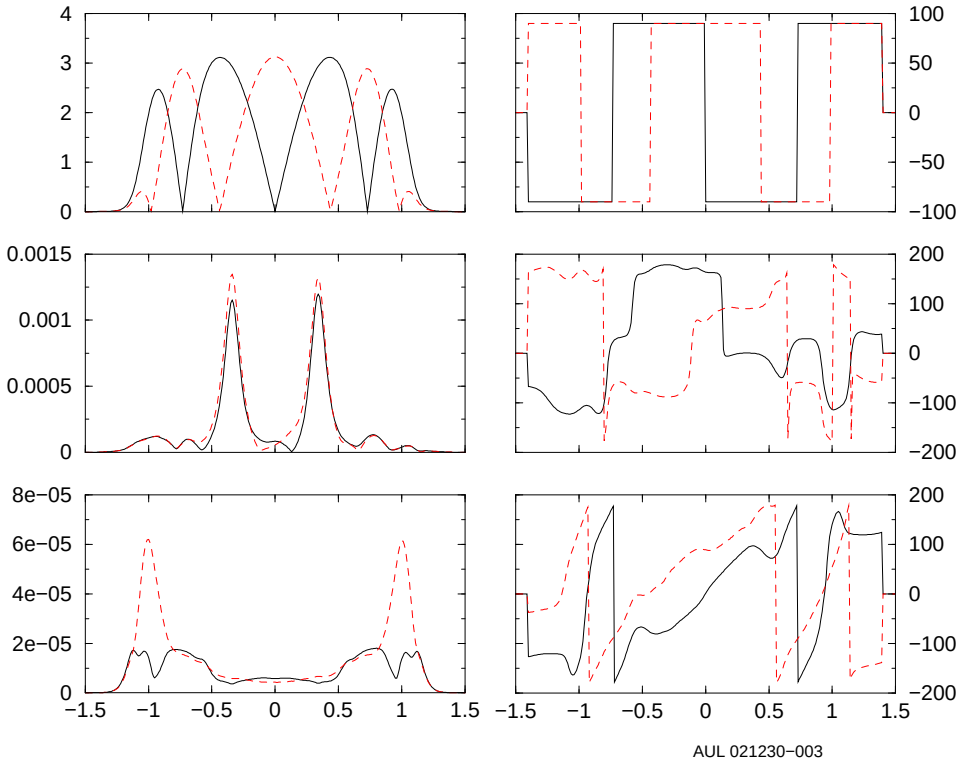


Figure 25: FFT analysis of the field on a 1 mm radius circle around the axis. First row: dipole, 2.nd row: quadrupole, 3.rd row: sextupole. Left column: amplitude ($[T], [T/m], [T/m^2]$, respectively), rigth column: phase [deg]. Solid lines: $x$ quantities, dashed: $y$.

then perform an FFT analysis on the data. Results are shown in Fig. 25. It is in particular noteworthy the twin quadrupole amplitude peak corresponding to the two ends of the solenoid.

In order to decrease snake focusing, we attempted to correct field gradients along a trajectory. A complete correction with *ad hoc* multipoles in the snake is probably an academic exercise, as pointed out in sec. 5, because, even if it were successful, there is no much space for current carrying coils inside the snake. However, we will point out here to a possible strategy.

To calculate the field gradients along a trajectory, we moved from the reference trajectory at a given energy by a small amount in $x, y, z$. These gradients are shown in Figs. 26 and 27. The figures shows symmetries due to the Div and Curl conditions of Eq.(10), a confirmation that the *Opera3d* numerical map field is Maxwellian.

To correct these gradients, we tried to create analytical field maps to be superimposed on the *Opera-3d* maps. In particular, to correct the longitudinal

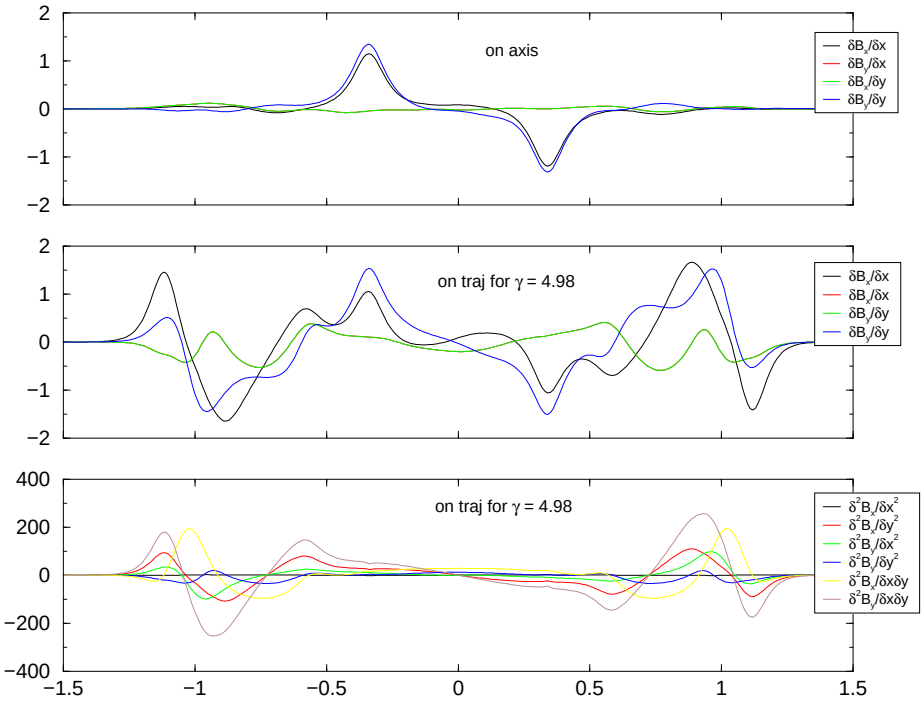


Figure 26: First $[T/m]$ and second $[T/m^2]$ derivatives of the field along a trajectory for $\gamma = 4.98$. No correction.

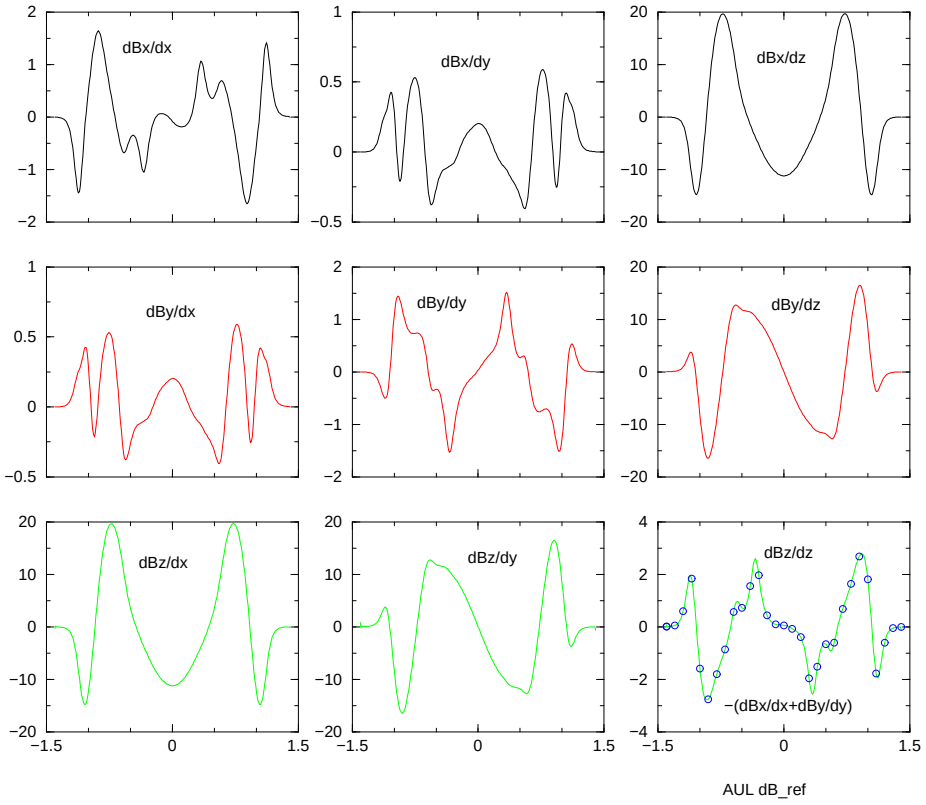


Figure 27: First Derivatives of the field along a trajectory for $\gamma = 4.98$. No correction

gradient of the longitudinal field $\partial B_z/\partial z$, we used solenoids, constructed from loops using Eq.(16) (see [10])

$$\vec{B} = \frac{\mu I}{2\pi}\vec{b}, \quad \begin{cases} b_\rho = \frac{z}{\rho\sqrt{\Delta}}\left[-K(m) + \frac{f_1}{f_2}E(m)\right] \\ b_z = \frac{1}{\sqrt{\Delta}}\left[K(m) + \frac{f_3}{f_2}E(m)\right] \\ b_x = b_\rho \cos\phi \\ b_y = b_\rho \sin\phi \end{cases} \tag{16}$$

with

$$\begin{cases} \Delta = (a+\rho)^2 + z^2 & & \\ f_1 = a^2 + \rho^2 + z^2, & f_2 = (a-\rho)^2 + z^2, & f_3 = a^2 - \rho^2 - z^2 \\ m = 4a\rho/\Delta, & \phi = \arctan y/x, & \rho^2 = x^2 + y^2 \end{cases}$$

Gradients are

$$\begin{cases} \frac{\partial K(m)}{\partial m} = \frac{1}{2m}\left[\frac{E}{1-m} - K\right] \\ \frac{\partial E(m)}{\partial m} = \frac{1}{2m}\left[E - K\right] \end{cases} \tag{17}$$

then, after some algebra, obtain

$$\frac{\partial b_z}{\partial z} = \frac{z}{\Delta\sqrt{\Delta}}\left\{\frac{f_2}{f_1}K(m) - \left[1 - 2\frac{f_2}{f_1} - \left(1 + \frac{f_2}{f_1}\right)\frac{8a^2\rho^2}{f_1 f_2}\right]E(m)\right\} \tag{18}$$

A long solenoid has a quasi uniform $B_z$ field for its entire length and a radial field at both ends. The longitudinal gradient of this field is zero in the body of the solenoid and shows two peaks, of opposite signs at the ends. If we examine the longitudinal gradient in the snake witn the coupling solenoid described earlier, it shows at least three pairs of such gradient peaks (however, the middle ones are due to the added solenoid), and in principles they may be corrected with three solenoid. This correction is shown in Fig. 28. The longitudinal gradients have been flattened, as show by Fig. 29

To correct the transverse coupling gradient $\partial B_x/\partial y = \partial B_y/\partial x$, we used quadrupole fields as in Eqs.(19). For this correction we used thick quads with a Gaussian function of $z$ for $k_1$. The solenoidal field is Maxwellian, however the quad field is not. The field of a thin quadrupole of strength $k_1$ and tilt $\theta$ is

$$\begin{cases} \hat{B_x} = k_1 y,\ \hat{B_y} = k_1 x,\ \hat{B_z} = 0 \\ B_x = \hat{B_x}\cos\theta + \hat{B_y}\sin\theta \\ B_y = -\hat{B_x}\sin\theta + \hat{B_y}\cos\theta \\ B_z = 0 \end{cases} \tag{19}$$

with gradients

$$\begin{cases} \frac{\partial B_x}{\partial x} = k_1\sin\theta & \frac{\partial B_x}{\partial y} = k_1\cos\theta \\ \frac{\partial B_y}{\partial x} = k_1\cos\theta & \frac{\partial B_y}{\partial y} = -k_1\sin\theta \end{cases} \tag{20}$$

In the model we put quadrupoles in strategic positions, and a good flattening of the transverse gradients were achieved, as shown in Fig. 30 and 31.

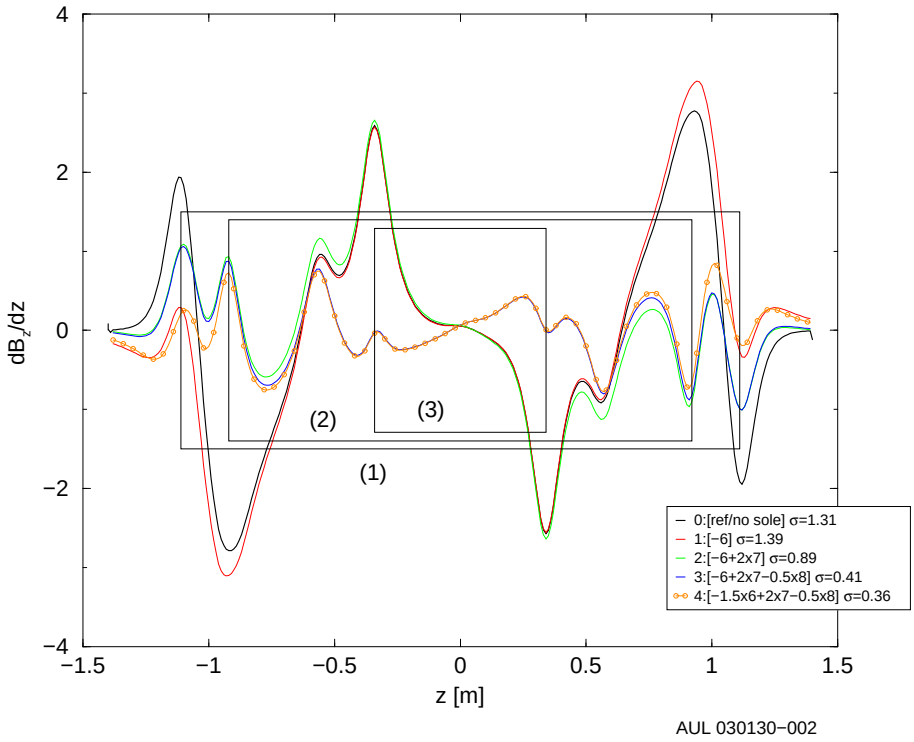


Figure 28: Correction of the longitudinal gradient by means of three solenoids.

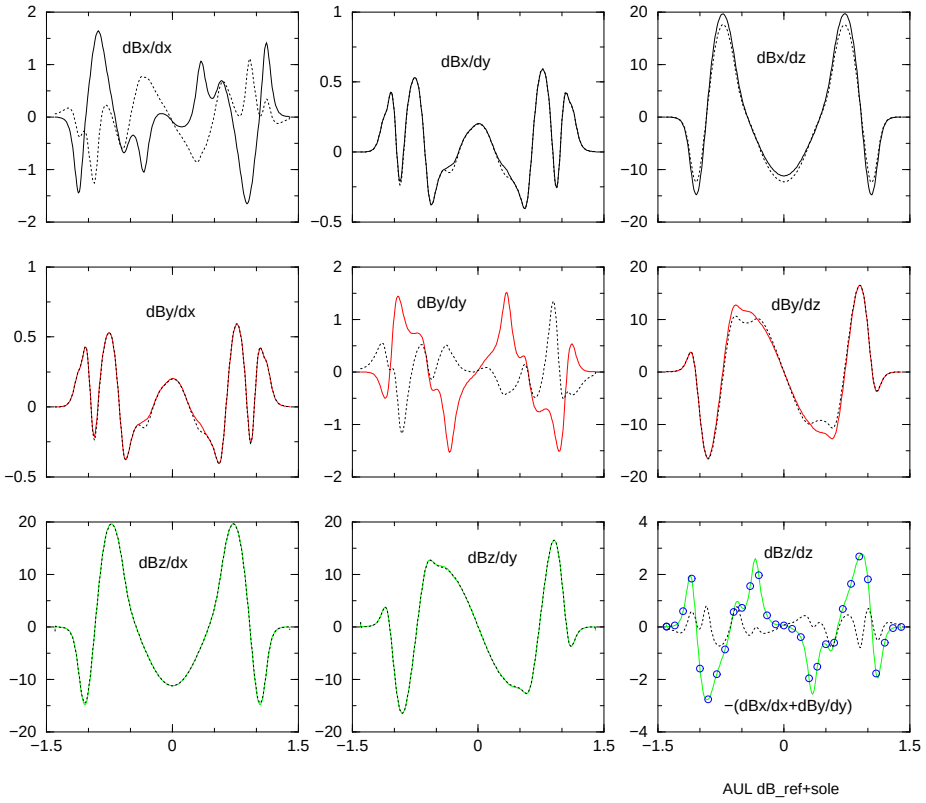


Figure 29: Derivatives of the field along a trajectory for $\gamma = 4.98$. Correct with solenoids

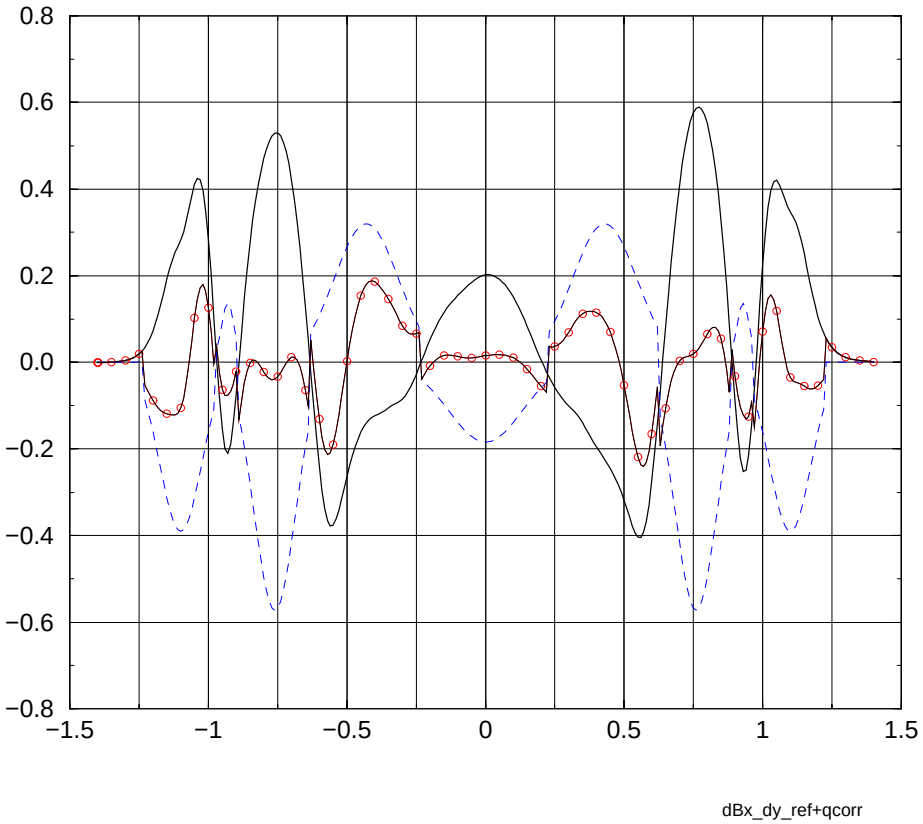


Figure 30: Derivative $\partial B_x/\partial y$ $[Tesla/m]$ along a trajectory for $\gamma = 4.98$. Correct with 9 quadrupoles. Solid line: no correction ($\sigma = 0.2376$). Dashed line: after correction ($\sigma = 0.08443$). Dashed line: gradient of correctors

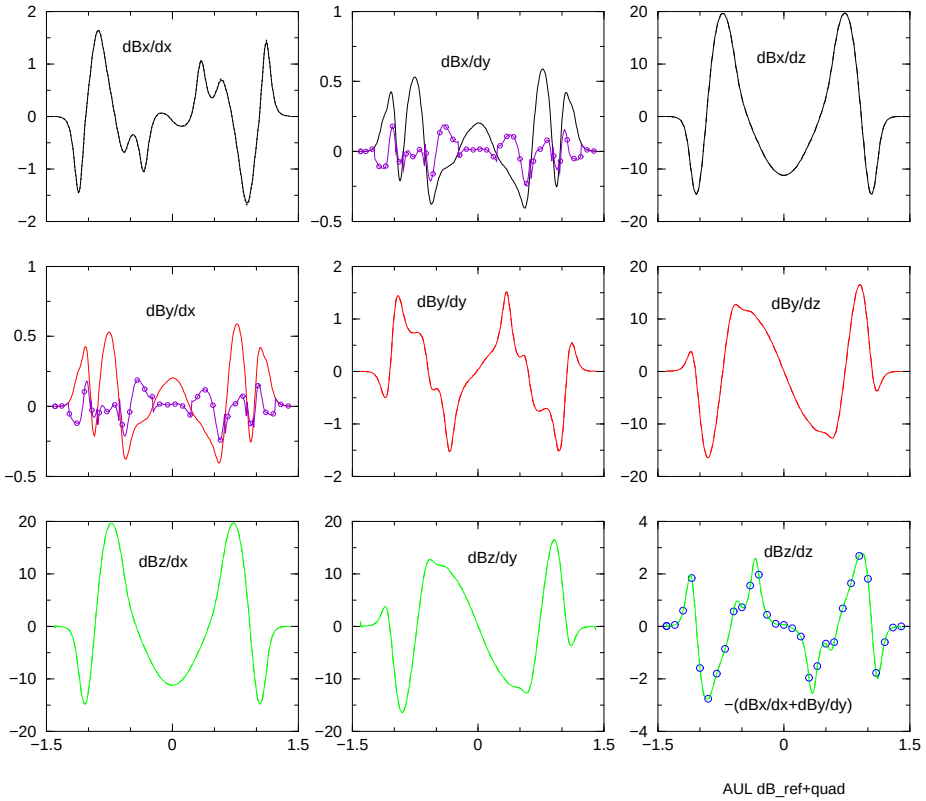


Figure 31: Derivatives of the field along a trajectory for $\gamma = 4.98$. Correct with quadrupoles

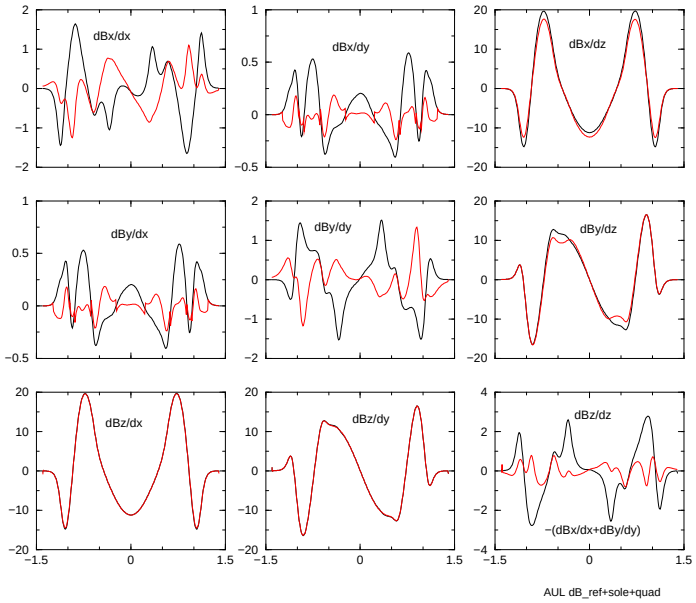


Figure 32: Derivatives of the field along a trajectory for $\gamma = 4.98$. Correct with solenoids and quadrupoles

.

Finally, putting both solenoids and quads, the correction achieved is shown in Fig. 32.

Values of the integrated field gradients for the four cases: (1) reference snake, (2) reference plus solenoid correction, (3) ref. plus quadrupole correction, and (4) ref. plus solenoid and quad correction, are shown in Table 14. Gradient integrated along the structure for different kind of corrections are shown in Table 15.

Table 14: Standard deviation of derivatives along the orbit with $\gamma = 4.98$ before/after correction

| | | | | | |
|---|---|---|---|---|---|
| $\frac{\partial B_x}{\partial x}$ : | 0.707/0.463, | $\frac{\partial B_x}{\partial y}$ : | 0.238/0.082, | $\frac{\partial B_x}{\partial x}$ : | 9.778/8.968, |
| $\frac{\partial B_y}{\partial x}$ : | 0.238/0.082, | $\frac{\partial B_y}{\partial y}$ : | 0.682/0.395, | $\frac{\partial B_y}{\partial x}$ : | 8.418/7.975, |
| $\frac{\partial B_z}{\partial x}$ : | 9.779/9.706, | $\frac{\partial B_z}{\partial y}$ : | 8.421/8.399, | $\frac{\partial B_z}{\partial x}$ : | 1.314/0.357 |

Table 15: Gradient Integrals $\gamma = 4.98$ before and after correction

Gradient Integrals: (over $1\mu m$)

| | | | |
|---|---|---|---|
| REF | | | |
| | -0.0039340 | 0.1977703 | 0.0278749 |
| | 0.1975422 | 0.0040224 | -0.0026021 |
| | 0.0272314 | -0.0017929 | 0.0002501 |
| REF+QUAD | | | |
| | -0.0023576 | -0.0038274 | 0.0280241 |
| | -0.0040277 | 0.0025411 | -0.0026004 |
| | 0.0226529 | -0.0016482 | 0.0002771 |
| REF+SOLE | | | |
| | -0.0015040 | 0.1826962 | -0.9952797 |
| | 0.1827635 | 0.0053172 | 0.0495957 |
| | -0.0068962 | -0.0006370 | -0.0031723 |
| REF+SOLE+QUAD | | | |
| | 0.0003914 | -0.0185830 | -1.0029469 |
| | -0.0187026 | 0.0045929 | 0.0422653 |
| | -0.0229668 | -0.0000232 | -0.0070449 |

# 8 Conclusions

A coordinated team effort has brought to the design of a super conducting snake for the AGS to improve the spin polarization of the extracted proton beam. Due to the limited space available, the snake would condense many functions in a very compact size. We succeeded in a design that produce a high degree of spin rotation and acceptable orbits. Coupling, that is an intrinsic property of the structure has been reduced, however we could not find any practical solution to correct focusing and integrated multipoles with a modification of the structure of the snake. We tried to point to a solution, but at this point we are inclined to believe that will be very hard to find a solution whitout recourse to machine elements somewhere else in the AGS magnetic lattice.

The snake, especially at injection energy, produces a strong deformation of the AGS optics. Following the work of E.Courant [11], we have a solution for matching the cold snake to the AGS lattice.. Details of these latter calculations will be presented in an upcoming report.

The snake is under construction. We keep our finger crossed.

# References

[1] Ya.S.Derbenev and A.M.Kondratenko. *Sov. Physics. Doklady*, 20:562, 1976.

[2] V.I.Ptitsyn and Yu.M.Shatunov. In: *Proc Third Workshop on Siberian Snakes and Spin Rotators*, BNL-52453, 15. Brookhaven National Laboratory. Upton, NY, Sept.12-13 1994.

[3] T.Roser, M.Syphers, E.Courant L.Ratner M.Okamura: *Helical Partial Snake for the AGS*. Technical Report AGS/RHIC/SN 072, Brookhaven National Laboratory. Upton, NY, March 19 1998.

[4] Vector Fields, Ltd: *Opera-3d Reference Manual*. Technical report, England, January 2002.

[5] R.Gupta, A.Luccio, G.Morgan W.Mackay K.Power T.Roser E.Willen M.Okamura: *Magnetic design of a super conducting AGS snake*. In: *Particle Accelerator Conference*, paper:WPAE002, Portland, Oregon, 2003.

[6] M.Okamura, T.Katayama, T.Tominaka T.Ohkawa R.Gupta A.U.Luccio W.W.MacKay T.Roser E.Willen: *Design of a partial snake for the AGS*. In: *European Particle Accelerator Conference*, EPAC2002, 2421, Paris, France, 3-7 June 2002.

[7] Blewett, J.P. and R.Chasman. *Journal of Appl. Physics*, 48:2692, 1977.

[8] A.U.Luccio: *Numerical Optimization of Siberian Snakes and Spin Rotators for RHIC*. In: *Trends in Collider Spin Physics*, 244, Trieste, Italy, 5-8 Dec 1995. World Scientific.

[9] A.U.Luccio: *Angles from Spin Matrices*. Technical Report AGS/RHIC/SN No. 03, Brookhaven National Laboratory. Upton, NY, October 8 1996.

[10] W.R.Smythe: *Static and Dynamic Electricity*. McGraw Hill, New York, 3.rd ed. 1968.

[11] E.D.Courant: *Matching Quadrupoles for AGS Helical Snake*. In: *SPIN2002 15.th International Spin Physics Symposium, Upton, NY, 9-14 Sept. 2002, AIP Conference Proceedings*, volume 675, 799–803.